Escaping from multiple visual threats: Modulation of escape responses in Pacific staghorn sculpin (*Leptocottus armatus*)

Hibiki Kimura[1,*], Tilo Pfalzgraff[2], Marie Levet[3], Yuuki Kawabata[1], John F. Steffensen[4], Jacob L. Johansen[5], Paolo Domenici[6]

[1]Graduate School of Fisheries and Environmental Sciences, Nagasaki University, 1-14 Bunkyo-machi, Nagasaki, Japan.

[2]Technical University of Denmark, DTU AQUA, Section for Aquaculture, The North Sea Research Centre, 9850 Hirtshals, Denmark.

[3]Département de Sciences Biologiques, Université de Montréal, Campus MIL, 1375 Avenue Thérèse-Lavoie-Roux, Montréal QC H2V 0B3, Canada

[4]Marine Biological Section, Department of Biology, University of Copenhagen, Strandpromenaden 5, DK-3000, Helsingør, Denmark

[5]Hawaii Institute of Marine Biology, University of Hawaii at Manoa, 46-007 Lilipuna Rd, Kaneohe, HI 96744, USA

[6]CNR–IBF, Institute of Biophysics, Pisa, Italy

***Corresponding author:** h.kimura787@gmail.com

SUMMARY STATEMENT

Using double stimulation from opposite sides at different time intervals to simulate coordinated predatory attacks, Pacific staghorn sculpin escape away from the first stimulus, but were unable to turn away from the second stimulus while the escape response was in progress.

KEYWORDS: C-start, escape response, looming stimuli, Pacific staghorn sculpin, predation, visual stimuli

ABBREVIATIONS: AIC, Akaike's Information Criterion; ALT, apparent looming threshold; ANOVA, analysis of variance; CM, center of mass; EM, expectation-maximization; GMD, Gaussian mixture distribution; I-T, information-theoretical; SD, standard deviation

ABSTRACT

Fish perform rapid escape responses to avoid sudden predatory attacks. During escape responses, fish bend their bodies into a C-shape and quickly turn away from the predator and accelerate. The escape trajectory is determined by the initial turn (Stage 1) and a contralateral bend (Stage 2). Previous studies have used a single threat or model predator as a stimulus. In nature, however, multiple predators may attack from different directions simultaneously or in close succession. It is unknown whether fish are able to change the course of their escape response when startled by multiple stimuli at various time intervals. Pacific staghorn sculpin (*Leptocottus armatus*) were startled with a left and right visual stimulus in close succession. By varying the timing of the second stimulus, we were able to determine when and how a second stimulus could affect the escape response direction. Four treatments were used: a single visual stimulus (control); or two stimuli coming from opposite sides separated by a 0 ms (simultaneous treatment); a 33 ms; or a 83 ms time interval. The 33 ms and 83 ms time intervals were chosen to occur shortly before and after a predicted 60 ms visual escape latency (i.e. during Stage 1). The 0 ms and 33 ms treatments influenced both the escape trajectory and the Stage 1 turning angle, compared to a single stimulation, whereas the 83 ms treatment had no effect on the escape trajectory. We conclude that Pacific staghorn

sculpin can modulate their escape trajectory only between stimulation and the onset of the response, but that escape trajectory cannot be modulated after the body motion has started.

INTRODUCTION

Fish avoid predators by performing sudden accelerations, i.e. fast start escape responses (Domenici and Blake, 1997). The kinematics and neural control of escape responses have been widely investigated (Domenici and Blake, 1993; Domenici and Hale, 2019; Eaton et al., 2001; Stewart et al., 2014). Fish escape responses typically consist of C- or S- starts, based on the shape of the fish at the end of the first contraction (Domenici and Hale, 2019). In C-starts, fish bend their bodies into a C-shape during the initial muscle contraction (Stage 1) usually away from the threat, while a subsequent return flip of the tail (when present, Domenici and Hale, 2019) can produce further acceleration (Stage 2) (Fleuren et al., 2018).

Fish can be startled using a variety of stimuli, from mechano-acoustic to tactile and visual stimuli (Domenici and Hale, 2019). The shortest latencies are typically associated with the stimulation of the mechano-acoustic sensory system leading to the activation of the Mauthner cells (M-cells) (Korn and Faber, 2005), whereas visual stimuli tend to show longer latencies because of the longer neural pathway (Mirjany and Faber, 2011) from the optic nerve to the M-cell via the optic tectum (Temizer et al., 2015). Mauthner cell ablation was shown to delay the escape response and to decrease survival in predator–prey encounters (Hecker et al., 2020).

Most previous studies on fish escape responses have focused on a single threat such as a model or a real predator approaching, resulting in an escape response directed away from the threat (Domenici and Blake, 1993; Stewart et al., 2013; Stewart et al., 2014; Walker et al., 2005). However, in nature, multiple predators may attack prey from two or more directions simultaneously or in close succession (Amo et al., 2004; Bshary et al., 2006; Stander, 1992;

Steinegger et al., 2018). Multiple co-occurring threats are known to affect the prey's escape directions; for example, lizards escape at ~180 degree away from single predators but at perpendicular to the predators when attacked simultaneously from two opposite directions (Cooper et al., 2007).

Previous work has investigated the possibility that a modification of the escape trajectory can occur after initial stimulation. Importantly, inhibition of the mechanosensory input occurs during Stage 1 in both C- and S- starts (Russell, 1976), leading Eaton et al. (1981) and Eaton and Emberley (1991) to suggest that the neural command underlying the escape response is ballistic once the movement has begun (i.e. without further sensory information to compute its trajectory). Indeed, Eaton et al. (1988) found that the Stage 2 command of the goldfish is preprogrammed and not dependent on sensory feedback, however it remains unknown if sensory feedback can occur before or after the initiation of Stage 1.

Some taxa are able to modulate escape responses to multiple successive attacks. Certain crickets, for instance, were found to use two escape modes (i.e. running and jumping) with different degrees of flexibility: when crickets escape through running from an initial predator attack, they were able to modulate their trajectory in response to a second attack. However, this was not that case for crickets which escaping by jumping from the initial attack (i.e. a ballistic response) (Sato et al., 2019). In fish, recent work has shown that larval zebrafish may be able to integrate sensory information from multiple threats during delayed escape responses due to a cluster of 38 prepontine neurons that are not part of the fast escape neural pathway (Marquart et al., 2019). This finding suggests that during the initial escape latency (i.e. before the onset of Stage 1 contraction), fish may have the potential to integrate sensory information from multiple threats. Additionally, Domenici and Blake (1993) suggested that sensory feedback may occur after the onset of Stage 1, resulting in a correction of escape trajectories during Stage 2. Hence, the extent of Stage 2 may, at least in part, be controlled by a feedback system (Domenici and Blake, 1993).

Here, we investigated the possibility that escape kinematics may vary depending on the time difference between the two visual threat stimuli coming from opposite sides. Visual looming stimuli are known to trigger an escape response once a given threshold (that depends on the size and speed of the approaching object) is reached (Cade et al., 2020; Hein et al., 2018). We hypothesize that if the escape response is fully ballistic from the time of the first stimulation, escape kinematics will not be modified by a second stimulus delivered at any time interval > 0 ms after the first one. If, in contrast, escape kinematics is modified by a second stimulus, this indicates that sensory feedback is possible during that time interval.

MATERIALS AND METHODS

Ethics statement

All animal care and experimental protocols followed the guidelines of the Institutional Animal Care and Use Committee at the University of Washington, Seattle, WA, USA (Protocol No. 4238-03).

Model species and housing conditions

Pacific staghorn sculpin [*Leptocottus armatus*; 13.9 ± 1.71 cm total length (TL); mean ± standard deviation (s.d.); n = 71] were captured by beach seining at Jackson Beach, south of San Juan Island, Washington, USA (48°31’11” N, 123°0’45” W) in July 2019. The fish were maintained in two acrylic tanks (87 cm length × 57 cm width × 14 cm depth) with flow-through seawater under a 14/10 h light/dark photoperiod, at 12.5 ± 0.5 °C (mean ± s.d.). They were acclimatized for ≥ 24 h and fed shrimp pieces every second day. At the end of the experiment, they were released at Jackson Beach.

Experimental setup

Experiments were conducted in an acrylic fish tank (125.5 cm length × 57 cm width × 35 cm depth; Fig. 1A) filled with seawater at 12.5 ± 0.5 °C (mean ± s.d.). White plastic panels were placed on the tank walls and bottom. A white plastic panel with grid lines (48 cm × 34 cm) was placed at the bottom center of the tank. Two 300 W halogen lamps were set above the tank to illuminate it. A high-speed camera (640 × 360 pixels, 240 fps; Stylus TG-870; Olympus Corp., Tokyo, Japan) was positioned 110 cm above the tank and recorded the escape response.

Two looming stimuli were used. Each stimulus was played on separate screens (1,600 × 1,200 pixels, 60 Hz; DELL 2000FP; Dell Inc., Round Rock, TX, USA) placed centrally on opposing sides of the experimental tank (Fig. 1A). Each stimulus simulated a black disk (24 cm diameter) approaching from 200 cm distances at a constant velocity of 1 m s^{-1}. The movie of the looming stimulus (1,600 × 1,200 pixels; 60 fps) was created with R v. 3.6.1 (R Core Team, 2019) using the package *loomeR* v. 0.3.0 (Carey, 2019). To control the delay of one movie from the other, two movies were stitched together horizontally using Shotcut Video Editor v. 19.07 (Meltytech LLC, Walnut Creek, CA, USA) and each side of the movie was played on a separate screen by the extended dual display mode. For the 0 ms treatment, two identical movies were stitched together and played simultaneously. For the 33 ms treatment, one of two movies (second stimulus) was played with a delay of two frames (~33 ms) relative to the first stimulus. For the 83 ms treatment, the second stimulus was played with a delay of five frames (~83 ms). For the control, only one single looming stimulus was played. The side of the first stimulus was randomized. The times for the delayed stimuli (33 ms and 83 ms) were selected based on the estimated visual escape latency of *L. armatus* (60 ms; Paglianti and Domenici, 2006). Hence, the stimulus delayed by 33 ms was assumed to be within the escape latency of *L. armatus* (defined as the time interval between the stimulus-reaching threshold and the fish response, corresponding to neurosensory

processing prior to the visible response; Paglianti and Domenici, 2006) (Fig. 2), whereas the stimulus delayed by 83 ms was assumed to occur during Stage 1 (Fig. 2).

Experimental procedure

Each fish was transferred to the experimental tank and placed in an opaque PVC shelter (15.5 cm diameter) where it was allowed to acclimatize for 15 min. A square panel under the tank bottom was used as a placement reference ensuring that all fish were placed in the center of the tank at a distance > 1.5 body lengths away from the walls to avoid any interference with their escape trajectory (Eaton and Emberley, 1991). The fish were placed perpendicular to the stimuli by carefully rotating the PVC shelter [86.76° ± 10.93° (mean ± s.d.); n = 66].

After acclimatization to the experimental tank, the shelter was removed and fish were left undisturbed for an additional two minutes, after which they were startled. Each fish was exposed to each of the four treatments (in random order) only once. The side of the first looming stimulus was randomly selected. Between stimuli, the fish were returned to the PVC shelter to avoid stimulation prior to each treatment. Fish were allowed over two minutes to recover from the previous stimulation before the next trial continued. If fish moved before the stimulation, fish were returned to the PVC shelter and were acclimatized for an additional two minutes. If its ventilation was higher than at rest (i.e. a sign of an elevated stress level) by our visual observation, extra time was allocated until the ventilation rate decreased before the next stimulus was played.

Data and statistical analysis

The 240fps video of the escape response was analyzed frame by frame with Logger Pro v. 3.15 (Vernier Software & Technology, Beaverton, OR, USA). The only responses used were those in which the fish reacted to the stimuli and initiated an escape response to the first

stimulus (total 66 responses: 0 ms treatment = 18 responses; 33 ms treatment = 13 responses; 83 ms treatment = 16 responses; control = 19 responses). The fish snout and center of mass [CM; 35% of total body length (Paglianti and Domenici, 2006)] were digitalized in each frame.

A total of six biomechanical and five time-distance variables were then calculated (Dadda et al., 2010; Domenici and Ruxton, 2015). The escape trajectory (°) was calculated as the angle between the direction of the line passing through the CM and the snout at the end of Stage 2 and the virtual movement direction of the first stimulus (Fig. 1A); The Stage 1 turning angle (°) was the angle between the line passing through the CM and the snout at the onset of Stage 1 and the line passing through the CM and the snout at the onset of Stage 2 (Fig. 1B). Stage 1 was taken as the time interval between the onset of Stage 1 and the onset of Stage 2 (Stage 1 turning duration; ms); The Stage 1 turning rate (° s^{-1}) was calculated by dividing the Stage 1 turning angle by the Stage 1 turning duration; The Stage 2 turning angle (°) was the angle between the lines passing through the CM and the snout at the onset of Stage 2 and those at the end of Stage 2 (Fig. 1B). Stage 2 was taken as the time from the onset to the end of Stage 2 (Stage 2 turning duration; ms); The Stage 2 turning rate (° s^{-1}) was calculated by dividing the Stage 2 turning angle by the Stage 2 turning duration; The apparent looming threshold (ALT; rad s^{-1}) triggering the escape response was calculated using the following equation (Eqn. 1) (Dill, 1974):

$$\frac{d\alpha}{dt} = \frac{4VS}{4D^2 + S^2} \#(\text{Eqn. 1})$$

where D is the virtual distance between the nearest fish eye and the virtual object (cm), S is the size of the virtual object (24 cm virtual diameter), and V is the apparent speed of the approaching object (100 cm s^{-1}).

The time-distance variables [maximum acceleration (m s^{-2}); maximum speed (cm s^{-1}); and cumulative distance (cm)] were measured based on the CM displacement. These variables were evaluated between the onset of Stage 1 and the end of Stage 2. Maximum acceleration and maximum speed were calculated by first- and second-order differentiation, respectively, of the cumulative distance for the time series. A Lanczos five-point quadratic moving regression method (Lanczos, 1956) was applied to calculate these last two values.

The treatments of 11 variables were fitted one- to nine-component Gaussian mixture distributions (GMD) with equal and unequal variance (Total 17 GMD models) with an expectation-maximization (EM) algorithm. The most parsimonious probability distribution on each variable was chosen based on the lowest Akaike information criterion (AIC). Then, in all variables, a dominant normal distribution of GMD of each treatment was compared with that of control with Dunnett-corrected 95% confidence intervals (Dunnet, 1964). As a post-hoc test, three treatments (0 ms, 33 ms, 83 ms) were compared with each other using an information-theoretic (I-T) approach, which can be used for multiple comparisons between treatments, and have several advantages over conventional methods such as Tukey HSD (Burnham et al., 2011; Dayton, 1998; Sugiura, 1978). The I-T approach allows comparisons of models with differing distributions (e.g. Gaussian mixture distributions) (Domenici et al., 2008) and nesting/non-nesting (Halsey, 2019; Richards et al., 2011), and are robust to the fact that the distributions of some variables in our data were not unimodal (based on a visual assessment, Fig. S1). Our three treatments (0ms, 33ms and 83ms) allowed for 5 combinations of comparisons by categorizing each group as the same (=) or different ($\neq$) (e.g. 0 ms = 33 ms $\neq$ 83 ms, see Fig S2 for combination details). AIC was calculated with the following equation:

$$AIC = -2\log L + 2k \#(\text{Eqn. } 2)$$

where k is the number of parameters and $\log L$ is the model log-likelihood. For example, parameters of normal distribution are a mean and variance. Thus, k is 2. In the case of two-component GMD with unequal variance, this GMD has two independent normal distributions i.e. it has two means and two variances. To adjust the total probability to 100%, it also has a mixing probability. Thus, k is 5. In general, k was calculated with the following equation:

$$k = k_{gaussian} N_{group} + (N_{group} - 1) \#(\text{Eqn. } 3)$$

where $k_{gaussian}$ is the number of parameters of the GMD (see Table 1), N_{group} is the number of groups in the model (see Fig S2).

$$\log L = \sum \log L_{group} \#(\text{Eqn. } 4)$$

where $\log L_{group}$ is the log-likelihood of each pooled group. The data categorized in the same group were pooled to estimate $\log L_{group}$. For example, in a combination where "0 ms = 33 ms $\neq$ 83 ms", 0 ms treatment is not different from 33 ms treatment, but is different from 83 ms treatment, and the 33 ms treatment is different from 83 ms treatment. In that scenario, the data of 0 ms and 33 ms treatments were pooled to estimate the first $\log L_{group}$ and the second $\log L_{group}$ of 83 ms treatment data was estimated independently. Then, the two $\log L_{group}$ were summed up to calculate the AIC. In an extreme case where "0 ms = 33 ms = 83 ms", data from all three treatments were pooled to estimate the $\log L_{group}$ and AIC, whereas if "0 ms $\neq$ 33 ms $\neq$ 83 ms", the data of these three treatments were separately analyzed to estimate each $\log L_{group}$, and the $\log L_{group}$ of three treatments were summed up to calculate the AIC. The most parsimonious model on each of the 11 variables was then

chosen based on the lowest AIC. The AIC difference (⊿AIC) was calculated between the best model and all others. Potential models were those with ⊿AIC < 2 (Sugiura, 1978).

All estimations of the GMDs, comparisons with a control with Dunnett-corrected 95% confidence intervals, and the analysis of the I-T approach to find differences among treatments were performed in R v. 3.6.1 (R Core Team, 2019) with the *Mclust* v. 5.4.5 package (Scrucca et al., 2016). Because some complex models of each variable could not be calculated with the *Mclust* package due to a singularity in the covariance matrix (Scrucca et al., 2016), the analysis of the I-T approach was performed only on models that could be calculated. Although escape trajectories are circular variables which potentially span 360° (Domenici et al., 2011), most escape trajectories were distributed through a limited arc and the uniformity of the escape trajectories was not supported by Watson's goodness of fit test for a circular uniform distribution (U^2 test; 0 ms: $U^2 = 0.86$, $P < 0.01$, 33 ms: $U^2 = 0.54$, $P < 0.01$, 83 ms: $U^2 = 0.60$, $P < 0.01$, control: $U^2 = 0.79$, $P < 0.01$) and escape trajectories were not distributed around 360° (Fig. 3A). Therefore, the distributions and the difference between treatments were analyzed using linear statistics (estimation of the GMD and the analysis of the I-T approach) as suggested by Batschelet (1981). Calculations of variables and statistical analyses were performed in R v. 3.6.1 with the *circular* v. 0.4-93 package (Agostinelli and Lund, 2017).

RESULTS

The summary of the statistical analyses on the kinematic variables are shown in Tables 2, 3, S1, and S2. The escape trajectories, Stage 1 turning angle, Stage 1 turning duration, and Stage 1 turning rate of 0 ms and 33 ms treatments were significantly smaller than those of control, while those of 83 ms treatment were not significantly different from those of control (Table S1, Figs 3A and 3B). The Stage 2 turning rate of 33 ms and 83 ms

treatments were significantly lower than that of control, while that of 0 ms treatment was not significantly different from that of control (Table S1). The apparent looming threshold of 33 ms treatment was significantly higher than that of control. In contrast, the threshold of 0 ms and 83 ms treatments were not significantly different from that of control (Table S1). The cumulative distance of the 0 ms and 83 ms treatments were significantly shorter than that of the control (Table S1). The best model of Stage 2 turning rate in the I-T approach was "0 ms ≠ 33 ms = 83 ms", indicating that Stage 2 turning rate of 0 ms treatment was lower than those of 33 ms and 83 treatments. The best model of the apparent looming threshold was "33 ms ≠ 0 ms = 83 ms", indicating that 33ms treatment was lower than those of 0 ms and 83 ms treatments. The best models of the other variables were "0 ms = 33 ms = 83 ms", suggesting no differences in the treatments.

DISCUSSION

The escape trajectories of the staghorn sculpin differed between a single and dual threat stimuli when the fish were visually stimulated from the left and right sides within 33 ms of one another. The mean of the escape trajectories for a single threat stimulus in control was 110.60° (i.e. escaping away from a single threat stimulus). On the other hand, the escape trajectories for dual threat stimuli in the 0 and 33 ms treatments were nearly 90° (i.e. perpendicular to the line of attack of dual threat stimuli). Hence, when attacked from two sides simultaneously or with a short delay (33 ms) between dual threat stimuli, fish tended to escape along a "compromise" trajectory at a similar angle from both stimuli. However, the escape trajectories when the fish were attacked from two sides with a long delay (83 ms) between dual threat stimuli (i.e. when the delayed stimulus occurred after Stage 1 initiation) did not differ from the single stimulus treatment. Consequently, our findings suggest that the escape trajectory of staghorn sculpin is not fully ballistic and sensory feedback may occur

during the initial latency period of the escape responses. Once Stage 1 of the escape response is initiated, the escape trajectory is set and is not affected by further feedback control.

Behavioral and neurophysiological studies have shown that the Stage 1 turning angles are affected by stimulus direction (Domenici and Blake, 1993; Eaton and Emberley, 1991; Kimura and Kawabata, 2018). Stage 1 turning angles tend to be wide when the stimulus approaches fronting the prey and narrow when the stimulus approaches behind the prey (Domenici and Blake, 1993; Eaton and Emberley, 1991; Kimura and Kawabata, 2018). The optimal escape trajectory is suggested to range 90° and 180° depending on predator speed (Bhattacharyya et al., 2017; Domenici, 2002; Domenici et al., 2011; Weihs and Webb, 1984). Here, the fish were stimulated from the left and right sides. Thus, the resulting escape strategy consisted of remaining at an equal distance from both threats by escaping at 90° when the two stimuli were simultaneous. The results of the present study suggest that the fish minimize their Stage 1 turning angles when they are being attacked from the left and right sides simultaneously. Interestingly, control fish escaped at 110.60° (range 74.33 - 272.35°), which appears smaller than the mean escape trajectory (132°, range 98 - 175°) of the same species in the previous study (using a single visual stimulus with a same velocity to this study, but using a nearly square tank) (Paglianti and Domenici, 2006). The rectangular shape of our experimental tank or other unknown factors may have caused this difference.

The mechanism allowing the modulation of Stage 1 turning angles in the 0 ms and 33 ms treatments could be related to the activity of Mauthner cells and associated neurons, as well as the prepontine neurons (Marquart et al., 2019). Prepontine neurons facilitate the integration of multiple sensory information (visual and auditory) and alter Stage 1 of the escape response (Marquart et al., 2019). It is possible that a similar mechanism may occur in the presence of two visual stimuli; i.e. inputs from both eyes might be integrated by prepontine neurons before the onset of escape response. Additionally, the apparent looming threshold of 33 ms treatment was higher than the control, which corresponds to an

approximately 57 ms delay in the escape latency of the 33 ms treatment. This result suggests that when the fish perceives the second stimulus during the neural processing (i.e. between the first stimulation and the onset of Stage1), it delays the process based on the single stimulus and integrates the second stimulus information, resulting in 90° escape trajectory from both stimuli. Interestingly, this delay was not observed in the 0 ms treatment, suggesting that two simultaneous stimuli do not cause additional processing, although the mean escape trajectory is also nearly 90° (as in the 33 ms treatment), likely as a result of the symmetrical stimuli from both sides.

There were no differences among treatments in terms of their Stage 2 turning angles. In Stage 2, contraction of the body trunk muscles flips the caudal fin to the opposite side (Foreman and Eaton, 1993). As acceleration increases during Stage 2, the body slightly rotates, and the final escape direction is determined. The accelerations and propulsive forces and jets are stronger in Stage 2 than they are in Stage 1 (Fleuren et al., 2018; Tytell and Lauder, 2008; Voesenek et al., 2019), and they differ in terms of the relative importance of the rotation or acceleration (propulsion) to their movement (Domenici and Blake, 1993; Domenici et al., 2004; Eaton et al., 1977; Eaton and Hackett, 1984; Tytell and Lauder, 2008; Weihs, 1973). Escape trajectories are related to Stage 1 turning angles (Domenici and Hale, 2019) and the Stage 2 turning angles and rates are smaller than those of Stage 1 (Fleuren et al., 2018; Voesenek et al., 2019). Thus, Stage 2 plays a relatively more important role in acceleration than it does in escape trajectory. The limited effect of stage 2 on the escape trajectory is in line with the lack of differences in Stage 2 turning angles among treatments. Differences between treatments and control were found in cumulative distances, Stage 1 turning durations and rates and the Stage 2 turning rates. These may be related to the differences of the Stage 1 and 2 turning angles.

When the second stimulus reached its threshold after the initiation of the escape response (i.e. in the 83 ms treatment), there was no change in the escape trajectory compared to the control. This is in line with a study on fathead minnows attempting to escape tentacled snakes (Catania, 2009). When fathead minnows were at a strike distance, the tentacled snakes generated a water flow with their bodies and induced a C-start in the fish, directed away from their body but into the snake's mouth. Prey fish cannot modify their escape response after their reaction to the body-generated water flow because one of two Mauthner cells, which fires first, stimulates the body trunk muscle to initiate an escape response but inhibits activation of the opposite body trunk muscle (Faber et al., 1991; Korn and Faber, 2005). In the 83 ms treatment here, it is likely that the Mauthner cell on the stimulus side was activated, with feedback inhibition preventing the activation of the opposing Mauthner cell (Korn and Faber, 2005) as the latter would result in poor escape response performance. As a result, the escape trajectory of the 83 ms treatment did not differ from that of the control. However, our 33 ms treatment suggests that, if stimulated during the neural processing of the first stimulus (i.e. during the escape latency), fish can modify their escape trajectory. Hence, our results demonstrate that fish are capable of receiving additional sensory information during the neurosensory process that involves the circuitry from the optic tectum to the Mauthner cells (Zottoli et al., 1987).

In conclusion, we suggest that the escape response consists of a flexible phase (from the stimulation until onset of Stage 1) where sensory feedback is possible, and a ballistic phase (from the onset of Stage 1 onwards). The ballistic phase is likely to occur in fish fast escape responses as a result of inhibition of the Mauthner cell to trigger a further contraction during stage 1 (Faber et al., 1991). Specifically, a feed-forward inhibitory network guarantees that when one Mauthner cell is excited, (1) it only generates a single action potential (preventing repetitive firing of one Mauthner cell) and (2) the contralateral Mauthner cell will not be activated. As suggested by Faber et al. (1991), this prevents the occurrence of

ineffective escape behaviors, characterized by multiple fast body bends, and bilateral muscle contraction which would lead to minimal displacement of the fish. While such ineffective motion patterns are prevented, so is the integration of multiple threats within the time interval that corresponds to stage 1. Hence, effective escape is ensured at the cost of eliminating the flexibility that would be associated with sensory feedback during the early phase of the escape response.

We found that Pacific staghorn sculpin can modulate their escape response only between stimulation and the onset of the response, but that escape responses are ballistic after the body motion has started. Although a flexible phase of Pacific staghorn sculpin lasts for at least 33 ms after stimulation, other fish species may show a different relative timing of the flexible and ballistic phases. Identifying which patterns are employed and during which phase, may depend on the species and a phylogenetical analysis of escape flexibility would help us understand the evolution of fish escape response patterns. Furthermore, future research integrating behavioral experiments with neurophysiological measures (e.g. calcium imaging) could allow to understand how the behavioral patterns of the escape response are related to the neural activity when fish are startled by multiple threats.

ACKNOWLEDGEMENTS

We would like to thank the 2019 Fish Swimming course for support and assistance with fish collections, Friday Harbor Laboratories, University of Washington, for facilities and technical support. H.K. would like to thank his sponsor, Japan/U.S. – E.S. Morse Scholar Exchange Program and M.L. would like to thank the ‘Adopt a Student’ program, the Dudley Fund, and the GRIL (Interuniversity Research Group in Limnology and Aquatic Environments) for their financial support to attend the 2019 Fish Swimming course.

COMPETING INTERESTS

No competing interests to declare.

FUNDING

This study was funded by Grants-in-Aid for Scientific Research, Japan Society for the Promotion of Science, to Y.K. (19H04936). H.K. was supported by Japan/U.S. – E.S. Morse Scholar Exchange Program. M.L. was supported by the University of Washington and by a grant from the GRIL (an FRQNT funded strategic research network).

DATA AVAILABILITY

https://figshare.com/articles/dataset/dataframe_csv/19519033

AUTHOR CONTRIBUTIONS

Conceptualization: P.D.; Methodology: P.D., J.F.S., J.LJ.; Software; H.K.; Formal analysis; H.K., Y.K., T.P., M.L., P.D.; Investigation: H.K., T.P., M.L.; Resources: H.K., T.P., M.L., P.D., J.F.S., J.L.J.; Data Curation: H.K., T.P., M.L.; Writing – Original Draft: H.K.; Writing – Review & Editing: H.K., P.D., J.L.J., Y.K., M.L., T.P.; Visualization: H.K.; Supervision: P.D., Y.K.; Project administration: P.D.

REFERENCES

Agostinelli, C. and Lund, U. (2017). R package 'circular': Circular statistics (version 0.4-93). https://r-forge.r-project.org/projects/circular/ (accessed 2021-1-6).

Amo, L., López, P. and Martín, J. (2004). Multiple predators and conflicting refuge use in the wall lizard, *Podarcis muralis*. *Ann. Zool. Fenn.* **41**, 671-679.

Batschelet, E. (1981). Circular statistics in biology. New York: Academic Press.

Bhattacharyya, K., McLean, D. L. and MacIver, M. A. (2017). Visual threat assessment and reticulospinal encoding of calibrated responses in larval zebrafish. *Curr. Biol.* **27**, 2751-2762.e6.

Bshary, R., Hohner, A., Ait-el-Djoudi, K. and Fricke, H. (2006). Interspecific communicative and coordinated hunting between groupers and giant moray eels in the Red Sea. *PLOS Biol.* **4**, e431.

Burnham, K. P., Anderson, D. R. and Huyvaert, K. P. (2011). AIC model selection and multimodel inference in behavioral ecology: some background, observations, and comparisons. *Behav. Ecol. Sociobiol.* **65**, 23-35.

Cade, D. E., Carey, N., Domenici, P., Potvin, J. and Goldbogen, J. A. (2020). Predator-informed looming stimulus experiments reveal how large filter feeding whales capture highly maneuverable forage fish. *Proc. Natl. Acad. Sci. U.S.A.* **117**, 472-478.

Carey, N. (2019). loomeR: Looming animations for use in behavioural and neurological experiments. https://github.com/nicholascarey/loomeR (accessed 2021-1-6), https://doi.org/10.5281/zenodo.1212570 (accessed 2021-1-6).

Catania, K. C. (2009). Tentacled snakes turn C-starts to their advantage and predict future prey behavior. *Proc. Natl. Acad. Sci. U.S.A.* **106**, 11183.

Cooper, W. E., Pérez-Mellado, V. and Hawlena, D. (2007). Number, speeds, and approach paths of predators affect escape behavior by the balearic lizard, *Podarcis lilfordi*. *J. Herpetol.* **41**, 197-204.

Dadda, M., Koolhaas Wouter, H. and Domenici, P. (2010). Behavioural asymmetry affects escape performance in a teleost fish. *Biol. Lett.* **6**, 414-417.

Dayton, C. M. (1998). Information criteria for the paired-comparisons problem. *Am. Stat.* **52**, 144-151.

Dill, L. M. (1974). The escape response of the zebra danio (*Brachydanio rerio*) I. The stimulus for escape. *Anim. Behav.* **22**, 711-722.

Domenici, P. (2002). The visually mediated escape response in fish: Predicting prey responsiveness and the locomotor behaviour of predators and prey. *Mar. Freshw. Behav. Physiol.* **35**, 87-110.

Domenici, P., Blagburn, J. M. and Bacon, J. P. (2011). Animal escapology I: theoretical issues and emerging trends in escape trajectories. *J. Exp. Biol.* **214**, 2463-2473.

Domenici, P. and Blake, R. (1997). The kinematics and performance of fish fast-start swimming. *J. Exp. Biol.* **200**, 1165-1178.

Domenici, P. and Blake, R. W. (1993). Escape trajectories in angelfish (*Pterophyllum eimekei*). *J. Exp. Biol.* **177**, 253-272.

Domenici, P., Booth, D., Blagburn, J. M. and Bacon, J. P. (2008). Cockroaches keep predators guessing by using preferred escape trajectories. *Curr. Biol.* **18**, 1792-1796.

Domenici, P. and Hale, M. E. (2019). Escape responses of fish: a review of the diversity in motor control, kinematics and behaviour. *J. Exp. Biol.* **222**, jeb166009.

Domenici, P. and Ruxton, G. D. (2015). Prey behaviors during fleeing: escape trajectories, signaling and sensory defenses. In *Escaping from Predators: An Integrative View*

of Escape Decisions, pp. 199-224.

Domenici, P., Standen, E. M. and Levine, R. P. (2004). Escape manoeuvres in the spiny dogfish (*Squalus acanthias*). *J. Exp. Biol.* **207**, 2339-2349.

Dunnet, C. W. (1964). New table for multiple comparisons with a control biometrics. *Biometrics* **20**, 482-491.

Eaton, R. C., Bombardieri, R. A. and Meyer, D. L. (1977). The Mauthner-initiated startle response in teleost fish. *J. Exp. Biol.* **66**, 65-81.

Eaton, R. C., DiDomenico, R. and Nissanov, J. (1988). Flexible body dynamics of the goldfish C-start: implications for reticulospinal command mechanisms. *J. Neurosci.* **8**, 2758.

Eaton, R. C. and Emberley, D. S. (1991). How stimulus direction determines the trajectory of the Mauthner-initiated escape response in a teleost fish. *J. Exp. Biol.* **161**, 469-487.

Eaton, R. C. and Hackett, J. T. (1984). The role of the Mauthner cell in fast-starts involving escape in teleost fishes. In *Neural Mechanisms of Startle Behavior*, (ed. R. C. Eaton), pp. 213-266. Boston, MA: Springer US.

Eaton, R. C., Lavender, W. A. and Wieland, C. M. (1981). Identification of Mauthner-initiated response patterns in goldfish: Evidence from simultaneous cinematography and electrophysiology. *J. Comp. Physiol. A* **144**, 521 - 531.

Eaton, R. C., Lee, R. K. K. and Foreman, M. B. (2001). The Mauthner cell and other identified neurons of the brainstem escape network of fish. *Prog. Neurobiol.* **63**, 467-485.

Faber, D. S., Korn, H. and Lin, J. (1991). Role of medullary networks and postsynaptic membrane properties in regulating Mauthner cell responsiveness to sensory excitation. *Brain Behav. Evol.* **37**, 286-297.

Fleuren, M., van Leeuwen, J. L., Quicazan-Rubio, E. M., Pieters, R. P. M., Pollux, B. J. A. and Voesenek, C. J. (2018). Three-dimensional analysis of the fast-start escape response of the least killifish, *Heterandria formosa*. *J. Exp. Biol.* **221**, jeb168609.

Foreman, M. B. and Eaton, R. C. (1993). The direction change concept for reticulospinal control of goldfish escape. *J. Neurosci.* **13**, 4101.

Halsey, L. G. (2019). The reign of the p-value is over: what alternative analyses could we employ to fill the power vacuum? *Biol. Lett.* **15**, 20190174.

Hecker, A., Schulze, W., Oster, J., Richter, D. O. and Schuster, S. (2020). Removing a single neuron in a vertebrate brain forever abolishes an essential behavior. *Proc. Natl. Acad. Sci. U.S.A.* **117**, 3254.

Hein, A. M., Gil, M. A., Twomey, C. R., Couzin, I. D. and Levin, S. A. (2018). Conserved behavioral circuits govern high-speed decision-making in wild fish shoals. *Proc. Natl. Acad. Sci. U.S.A.* **115**, 12224-12228.

Kimura, H. and Kawabata, Y. (2018). Effect of initial body orientation on escape probability of prey fish escaping from predators. *Biol. Open* **7**.

Korn, H. and Faber, D. S. (2005). The Mauthner cell half a century later: A neurobiological model for decision-making? *Neuron* **47**, 13-28.

Lanczos, C. (1956). Applied analysis. Englewood Cliffs, NJ: Prentice-Hall.

Marquart, G. D., Tabor, K. M., Bergeron, S. A., Briggman, K. L. and Burgess, H. A. (2019). Prepontine non-giant neurons drive flexible escape behavior in zebrafish. *PLOS Biol.* **17**, e3000480.

Mirjany, M. and Faber, D. S. (2011). Characteristics of the anterior lateral line nerve input to the Mauthner cell. *J. Exp. Biol.* **214**, 3368.

Paglianti, A. and Domenici, P. (2006). The effect of size on the timing of visually mediated escape behaviour in staghorn sculpin *Leptocottus armatus*. *J. Fish Biol.* **68**, 1177-1191.

Richards, S. A., Whittingham, M. J. and Stephens, P. A. (2011). Model selection and model averaging in behavioural ecology: the utility of the IT-AIC framework. *Behav. Ecol. Sociobiol.* **65**, 77-89.

Russell, I. J. (1976). Central inhibition of lateral line input in the medulla of the goldfish by neurones which control active body movements. *J. Comp. Physiol. A* **111**, 335-358.

Sato, N., Shidara, H. and Ogawa, H. (2019). Trade-off between motor performance and behavioural flexibility in the action selection of cricket escape behaviour. *Sci. Rep.* **9**, 18112.

Scrucca, L., Fop, M., Murphy, T. B. and Raftery, A. E. (2016). mclust 5: Clustering, classification and density estimation using Gaussian finite mixture models. *R J.* **8**, 205-233.

Shifferman, E. and Eilam, D. (2004). Movement and direction of movement of a simulated prey affect the success rate in barn owl Tyto alba attack. *J. Avian Biol.* **35**, 111-116.

Stander, P. E. (1992). Cooperative hunting in lions: The role of the individual. *Behav. Ecol. Sociobiol.* **29**, 445-454.

Steinegger, M., Roche, D. G. and Bshary, R. (2018). Simple decision rules underlie collaborative hunting in yellow saddle goatfish. *Proc. Royal Soc. B* **285**.

Stewart, W. J., Cardenas, G. S. and McHenry, M. J. (2013). Zebrafish larvae evade predators by sensing water flow. *J. Exp. Biol.* **216**, 388-398.

Stewart, W. J., Nair, A., Jiang, H. and McHenry, M. J. (2014). Prey fish escape by sensing the bow wave of a predator. *J. Exp. Biol.* **217**, 4328-4336.

Sugiura, N. (1978). Further analysts of the data by akaike' s information criterion and the finite corrections. *Commun. Stat. Theory Methods* **7**, 13-26.

R Core Team. (2019). R: A language and environment for statistical computing. R Foundation for Statistical Computing, Vienna, Austria.

Temizer, I., Donovan, Joseph C., Baier, H. and Semmelhack, Julia L. (2015). A visual pathway for looming-evoked escape in larval zebrafish. *Curr. Biol.* **25**, 1823-1834.

Tytell, E. D. and Lauder, G. V. (2008). Hydrodynamics of the escape response in bluegill sunfish, *Lepomis macrochirus*. *J. Exp. Biol.* **211**, 3359-3369.

Voesenek, C. J., Pieters, R. P. M., Muijres, F. T. and van Leeuwen, J. L. (2019).

Reorientation and propulsion in fast-starting zebrafish larvae: An inverse dynamics analysis. *J. Exp. Biol.* **222**, jeb203091.

Walker, J. A., Ghalambor, C. K., Griset, O. L., McKenney, D. and Reznick, D. N. (2005). Do faster starts increase the probability of evading predators? *Funct. Ecol.* **19**, 808-815.

Weihs, D. (1973). The mechanism of rapid starting of slender fish. *Biorheology* **10**, 343-350.

Weihs, D. and Webb, P. W. (1984). Optimal avoidance and evasion tactics in predator-prey interactions. *J. Theor. Biol.* **106**, 189-206.

Zottoli, S. J., Marek, L. E., Agostini, M. A. and Strittmatter, S. L. (1987). Morphological and physiological survival of goldfish Mauthner axons isolated from their somata by spinal cord crush. *J. Comp. Neurol.* **255**, 272-282.

Figures and Tables

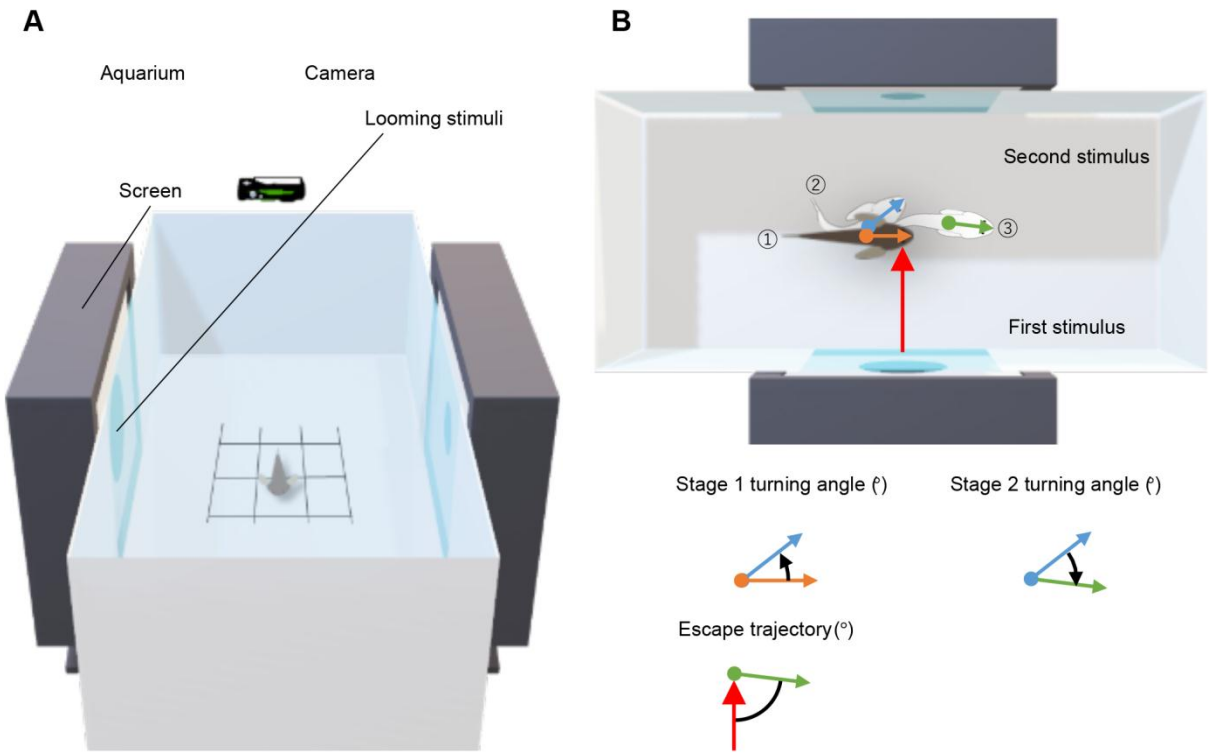

Fig. 1. (A) Schematic representation of experimental setup. Two screens were used to stimulate fish from the left and right sides with looming stimuli. Fish were always oriented parallel to the long axis of the aquarium (90° initial orientation). **(B) Definitions of Stage 1 and 2 turning angles and escape trajectory.** Upper diagram shows fish just before onset of escape response (1; brown fill), end of Stage 1 (2; white fill) and end of Stage 2 (3; white fill). Lower diagrams show variable definitions. Orange, blue, and green vectors represent fish directions just before onset of the escape response, at end of Stage 1, and end of Stage 2, respectively. Red arrow represents first stimulus direction. Each filled circle of arrows represents fish center of mass (CM).

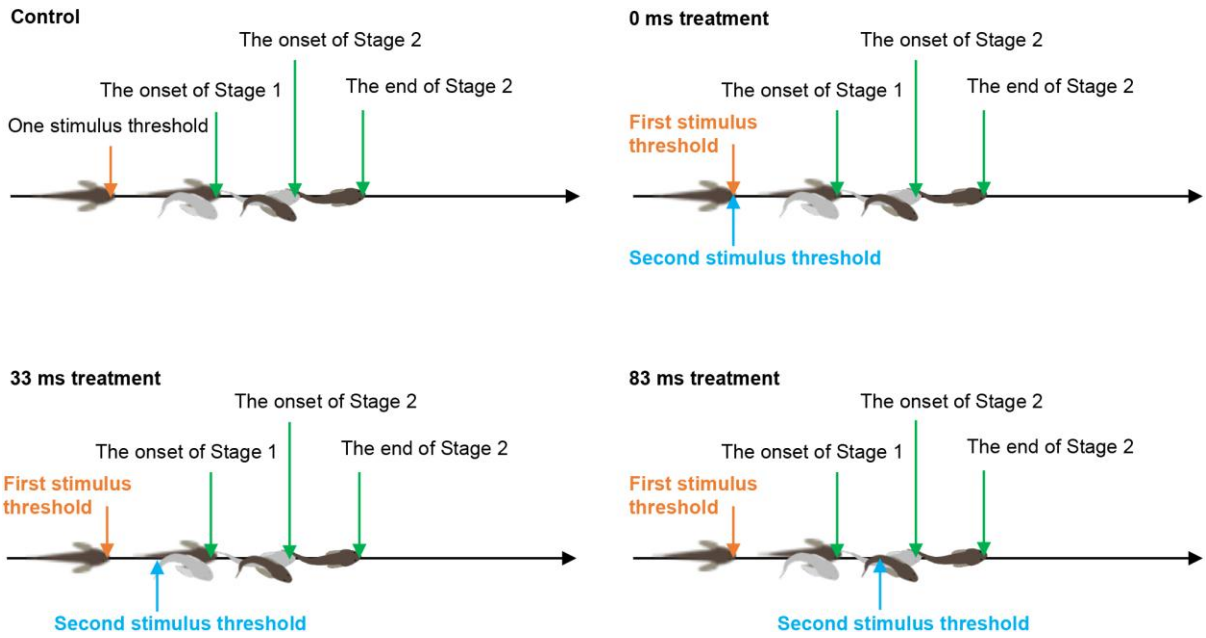

Fig. 2. Concepts of the four treatments. Diagrams show transitions of stimuli and fish responses for each treatment. Thresholds represent the onset of neural processing of the escape response.

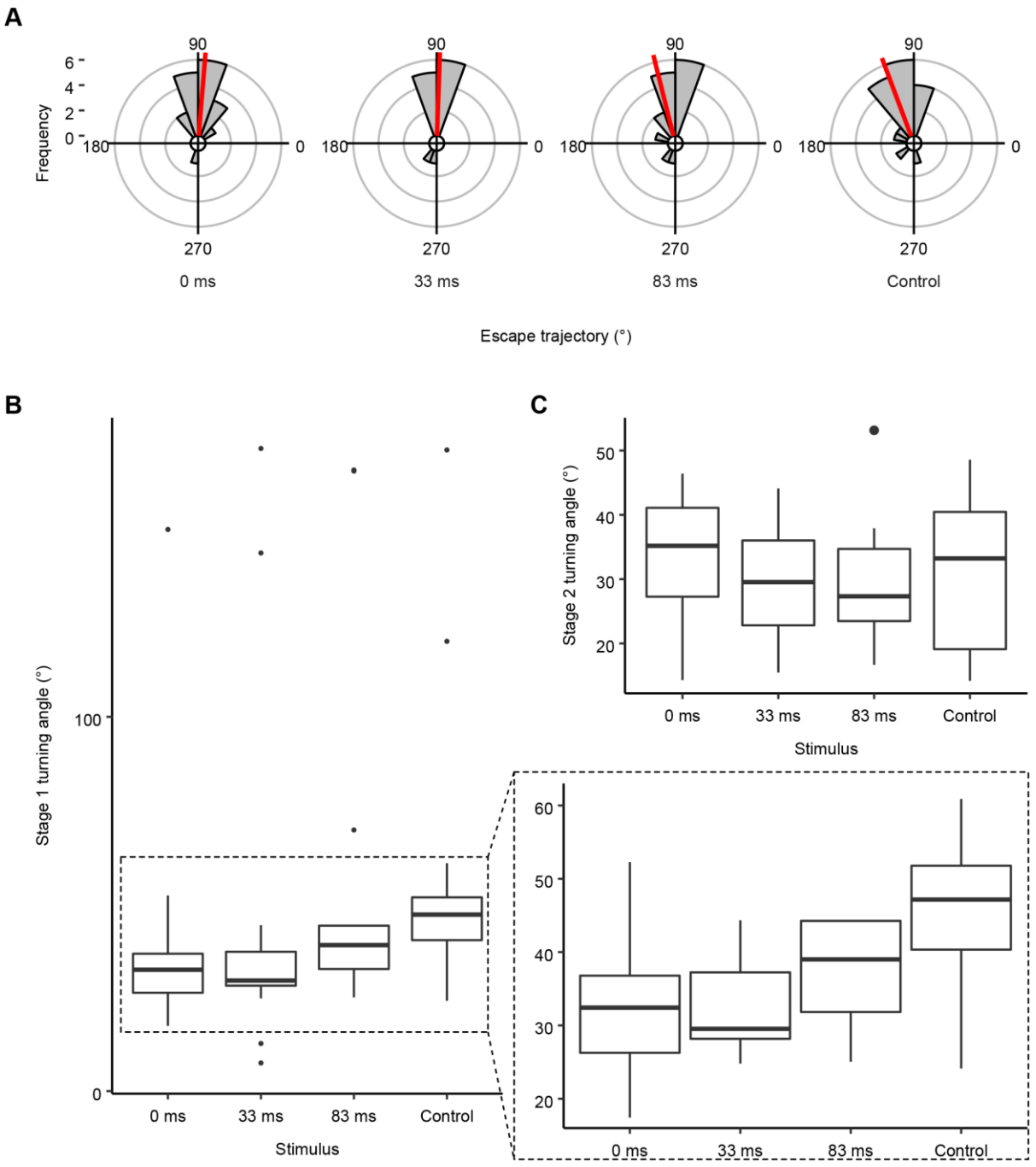

Fig. 3. (A) Circular histogram of escape trajectories. Red lines show circular mean value of each treatment. The bin intervals are 20°. The initial orientation of fish is 90°. **(B, C) Boxplots of Stage 1 turning angles excluded outliers (B) and Stage 2 turning angles (C).** Boxes represent median, lower, and upper quartiles. Ends of vertical lines are minima and maxima. Filled circles are values > 1.5× the upper quartile (outliers). (B) Stage 1 turning angles zoom in 16 – 63° is shown in the lower right panel.

Table 1. Models of Gaussian mixture distributions

No.	G	$V_{gaussian}$	$k_{gaussian}$
1	1	X	2
2	2	E	4
3	3	E	6
4	4	E	8
5	5	E	10
6	6	E	12
7	7	E	14
8	8	E	16
9	9	E	18
10	2	V	5
11	3	V	8
12	4	V	11
13	5	V	14
14	6	V	17
15	7	V	20
16	8	V	23
17	9	V	26

G, number of components of Gaussian mixture distribution; $V_{gaussian}$, model of variance of Gaussian mixture distribution; X = normal Gaussian distribution; E = Gaussian mixture distributions with equal variance; V = Gaussian mixture distributions with unequal variance; $k_{gaussian}$, number of parameters of Gaussian mixture distribution.

Table 2. The comparisons between each treatment and control on a dominant normal distribution with Dunnett-corrected 95% confidence intervals.

Variables	95% confidence intervals of a dominant normal distribution		
	0 ms - Control	33 ms - Control	83 ms - Control
Escape trajectories (°)	**-37.67 - -5.80**	**-38.46 - -2.51**	-22.20 - 11.33
Stage 1 turning angle (°)	**-23.00 - -5.79**	**-27.15 - -7.74**	-16.00 - 2.11
Stage 1 turning duration (ms)	**-12.01 - -1.84**	**-13.07 - -1.28**	-10.61 - 0.80
Stage 1 turning rate (° s^{-1})	**-665.34 - -27.70**	**-746.95 - -49.18**	-529.92 - 127.86
Stage 2 turning angle (°)	-5.41 - 12.07	-10.54 - 9.33	-10.16 - 9.15
Stage 2 turning duration (ms)	-10.92 - 4.98	-11.11 - 6.94	-10.45 - 7.11
Stage 2 turning rate (° s^{-1})	-261.86 - 63.48	**-726.62 - -364.25**	**-668.82 - -328.60**
Apparent looming threshold (rad s^{-1})	-2.79 - 1.98	**0.23 - 5.73**	-1.38 - 3.57
Maximum acceleration (cm s^{-2})	-1554.68 - 1667.15	-2156.13 - 1369.53	-1683.05 - 1640.58
Maximum speed (cm s^{-1})	-29.51 - 17.47	-35.59 - 15.83	-27.17 - 21.30
Cumulative distance (cm)	**-2.31 - -0.71**	-0.70 - 1.12	**-2.37 - -0.63**

Table 3. The results of information-theoretical approach analysis of each variable.

Variables	Model	k	$\log L$	G	$V_{gaussian}$	AIC	ΔAIC
Escape trajectories (°)	0 ms = 33 ms = 83 ms	4	-221.77	2	E	451.55	0.00
	0 ms = 83 ms≠33 ms	9	-217.10	2	E	452.21	0.66
	0 ms = 33 ms≠83 ms	9	-217.21	2	E	452.42	0.87
Stage 1 turning angle (°)	0 ms = 33 ms = 83 ms	6	-193.67	3	E	399.34	0.00
Stage 1 turning duration (ms)	0 ms = 33 ms = 83 ms	5	-195.56	2	V	401.13	0.00
Stage 1 turning rate (° s^{-1})	0 ms = 33 ms = 83 ms	2	-349.35	1	X	702.69	0.00
Stage 2 turning angle (°)	0 ms = 33 ms = 83 ms	2	-135.41	1	X	274.82	0.00
Stage 2 turning duration (ms)	0 ms = 33 ms = 83 ms	2	-131.08	1	X	266.16	0.00
Stage 2 turning rate (° s^{-1})	0 ms≠33 ms = 83 ms	9	-254.44	2	E	526.88	0.00
	0 ms = 33 ms≠83 ms	9	-254.75	2	E	527.50	0.62
Apparent looming threshold (rad s^{-1})	0 ms = 83 ms≠33 ms	17	-82.83	3	V	199.66	0.00
Maximum acceleration (cm s^{-2})	0 ms = 33 ms = 83 ms	2	-427.19	1	X	858.38	0.00
Maximum speed (cm s^{-1})	0 ms = 33 ms = 83 ms	2	-226.01	1	X	456.01	0.00
Cumulative distance (cm)	0 ms = 33 ms = 83 ms	5	-84.40	2	V	178.80	0.00

k, number of parameters of the model; $\log L$, log likelihood of the model; G, number of normal distributions of Gaussian mixture distribution; $V_{gaussian}$, model of variance of Gaussian mixture distribution; X = normal Gaussian distribution; E = Gaussian mixture distributions with equal variance; V = Gaussian mixture distributions with unequal variance; AIC, Akaike's information criterion; ΔAIC, the difference in AIC between each model and the best model. "0 ms", "33 ms" and "83 ms" show 0 ms treatment, 33 ms treatment and 83 ms treatment, respectively. "=" indicates that there is no different between left and right treatments. "≠" indicates there is a difference between left and right treatments. The best model has a ΔAIC value with zero. Each row only shows the results for ΔAIC < 2.

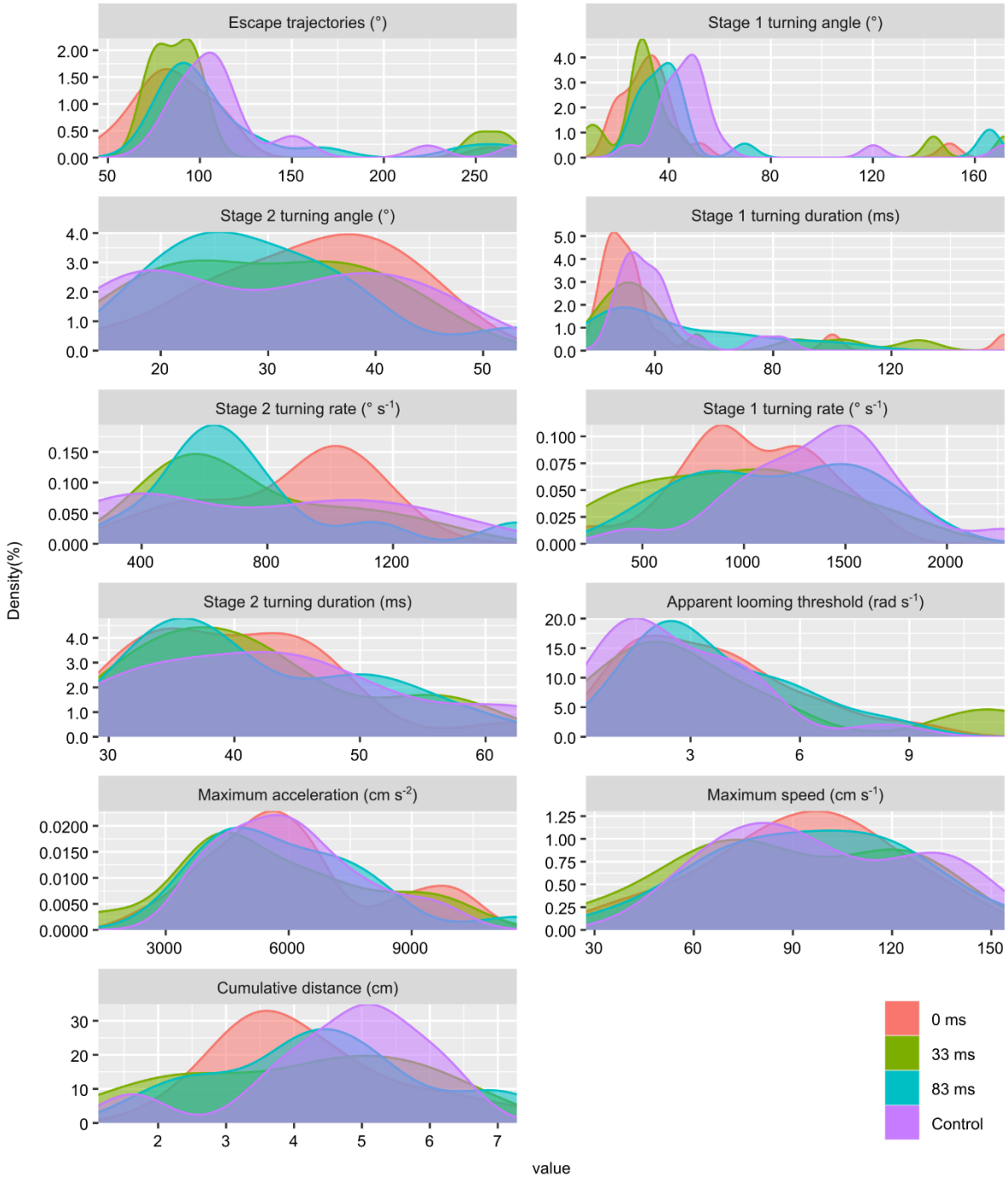

Fig. S1. Probability density curve of each variable. Red, green, blue and purple filled curves show 0 ms treatment, 33 ms treatment, 83 ms treatment and control's data, respectively.

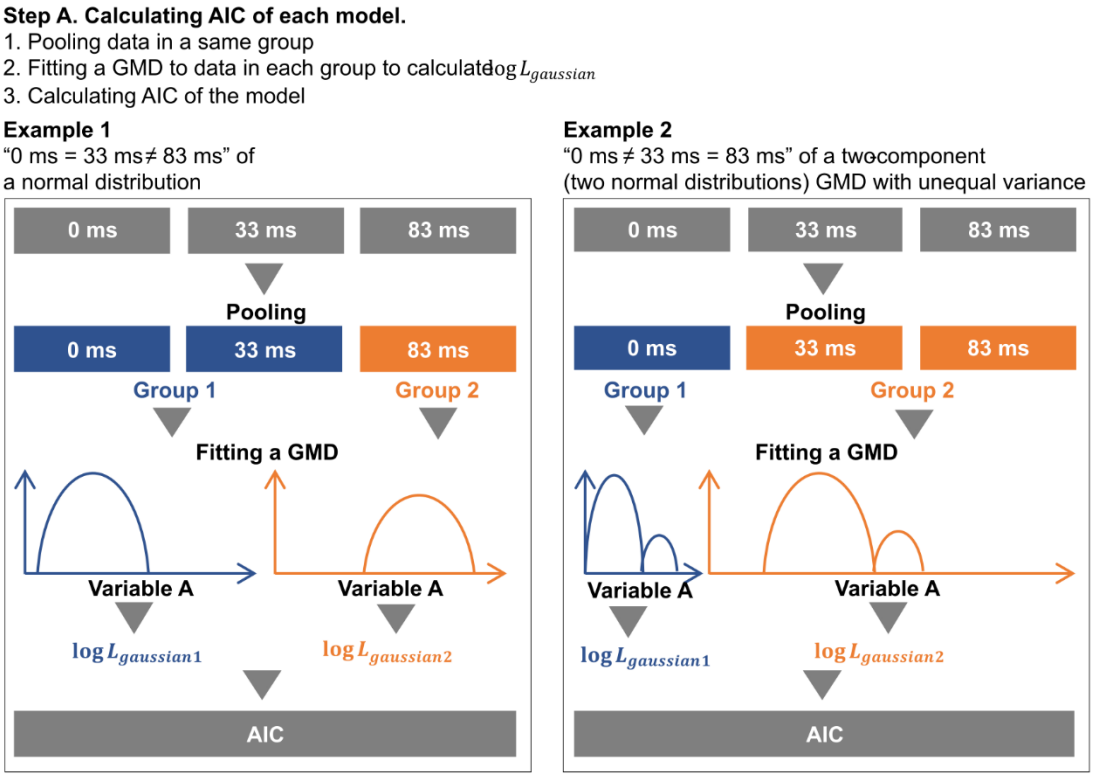

Step B. Comparing 5 models with AIC

No.	Model	N_{group}
1	0 ms = 33 ms = 83 ms	1
2	0 ms = 33 ms ≠ 83 ms	2
3	0 ms = 83 ms ≠ 33 ms	2
4	0 ms ≠ 33 ms = 83 ms	2
5	0 ms ≠ 33 ms ≠ 83 ms	3

Fig. S2. Graphical explanation of the information-theoretic approach to find the best fit model. AIC, Akaike information criterion; GMD, Gaussian mixture distribution; log L_{group}, log-likelihood of each pooled group; N_{group}, number of the groups; "0 ms", "33 ms" and "83 ms" show 0 ms treatment, 33 ms treatment, and 83 ms treatment, respectively. "=" indicates that there is no different between left and right treatments. "≠" indicates there is a difference between left and right treatments.

Table S1. Summary of best fitted Gaussian mixture distributions.

Variables	Treatments	Normal distribution 1			Normal distribution 2			Normal distribution 3		
		μ	σ^2	P_{mix}	μ	σ^2	P_{mix} (%)	μ	σ^2	P_{mix}
Escape trajectories (°)	0 ms	84.82	349.30	0.94	258.58	349.30	0.06			
	33 ms	86.07	104.29	0.85	257.60	104.29	0.15			
	83 ms	101.12	472.01	0.87	257.28	472.01	0.13			
	Control	106.55	417.87	0.89	248.10	417.87	0.11			
Stage 1 turning angle (°)	0 ms	31.10	73.56	0.49	31.10	73.56	0.46	150.06	73.56	0.06
	33 ms	28.05	112.85	0.43	28.04	112.85	0.42	157.73	112.85	0.15
	83 ms	38.55	98.47	0.44	38.54	98.47	0.43	165.80	98.47	0.13
	Control	45.50	130.43	0.46	45.50	130.43	0.44	145.74	130.43	0.11
Stage 1 turning duration (ms)	0 ms	28.39	27.31	0.81	95.28	2117.35	0.19			
	33 ms	30.42	52.25	0.77	106.93	293.89	0.23			
	83 ms	28.15	10.47	0.54	68.74	452.59	0.46			
	Control	35.32	38.18	0.84	70.61	173.23	0.16			
Stage 1 turning rate (° s^{-1})	0 ms	1025.55	118662.50	1.00						
	33 ms	974.00	203702.80	1.00						
	83 ms	1171.04	172961.70	1.00						
	Control	1372.06	156038.10	1.00						
Stage 2 turning angle (°)	0 ms	33.71	76.14	1.00						
	33 ms	29.77	85.78	1.00						
	83 ms	29.87	96.09	1.00						
	Control	30.37	127.19	1.00						
Stage 2 turning duration (ms)	0 ms	40.36	64.49	1.00						
	33 ms	41.25	77.95	1.00						
	83 ms	41.67	69.44	1.00						
	Control	43.33	106.02	1.00						
Stage 2 turning rate (° s^{-1})	0 ms	1022.97	14932.35	0.68	530.91	14932.35	0.32			
	33 ms	576.73	11385.53	0.70	1138.27	11385.53	0.30			
	83 ms	623.45	27492.06	0.83	1377.32	27492.06	0.17			
	Control	1122.16	24329.84	0.53	388.99	24329.84	0.47			
Apparent looming threshold (rad s^{-1})	0 ms	3.49	0.92	0.42	1.35	0.16	0.32	6.48	2.97	0.25
	33 ms	6.88	11.75	0.44	2.09	0.09	0.39	0.31	0.00	0.17
	83 ms	4.99	3.64	0.54	2.37	0.06	0.34	1.02	0.12	0.12
	Control	3.89	3.29	0.57	1.38	0.02	0.28	0.39	0.03	0.14
Maximum acceleration (cm s^{-2})	0 ms	6109.23	4392074.00	1.00						
	33 ms	5659.69	5371643.00	1.00						
	83 ms	6031.76	4088522.00	1.00						
	Control	6053.00	2855585.00	1.00						
Maximum speed (cm s^{-1})	0 ms	92.77	769.20	1.00						
	33 ms	88.91	1026.73	1.00						
	83 ms	95.86	862.47	1.00						
	Control	98.80	845.61	1.00						
Cumulative distance (cm)	0 ms	3.51	0.46	0.66	5.52	1.30	0.34			
	33 ms	5.23	0.66	0.62	2.21	0.44	0.38			
	83 ms	3.52	1.25	0.51	5.30	1.68	0.49			
	Control	5.02	0.69	0.89	1.62	0.00	0.11			

μ, the mean value of one of the normal distributions of the Gaussian mixture distribution; σ^2, the variance of one of the normal distributions of the Gaussian mixture distribution; P, the mixing probability of one of the normal distributions of the Gaussian mixture distribution; “0 ms”, “33 ms”, “83 ms” and “control” show 0 ms treatment, 33 ms treatment, 83 ms treatment, and control, respectively.

Table S2. Summary of the variables of each treatment.

Variables	0 ms	33 ms	83 ms	control
Escape trajectories (°)	85.29 ± 0.60 (*n* = 18)	87.96 ± 0.88 (*n* = 13)	103.98 ± 0.85 (*n* = 16)	110.60 ± 0.72 (*n* = 19)
Stage 1 turning angle (°)	37.71 ± 29.39 (*n* = 18)	48.00 ± 49.94 (*n* = 13)	54.45 ± 44.66 (*n* = 16)	56.05 ± 33.71 (*n* = 19)
Stage 1 turning duration (ms)	41.20 ± 34.44 (*n* = 18)	48.08 ± 35.26 (*n* = 13)	46.88 ± 25.80 (*n* = 16)	40.79 ± 15.31 (*n* = 19)
Stage 1 turning rate (° s^{-1})	1025.55 ± 354.46 (*n* = 18)	974.00 ± 469.76 (*n* = 13)	1171.04 ± 429.53 (*n* = 16)	1372.06 ± 405.84 (*n* = 19)
Stage 2 turning angle (°)	33.71 ± 9.01 (*n* = 16)	29.77 ± 9.76 (*n* = 10)	29.87 ± 10.28 (*n* = 11)	30.37 ± 11.67 (*n* = 15)
Stage 2 turning duration (ms)	40.36 ± 8.29 (*n* = 16)	41.25 ± 9.31 (*n* = 10)	41.67 ± 8.74 (*n* = 11)	43.33 ± 10.66 (*n* = 15)
Stage 2 turning rate (° s^{-1})	866.18 ± 268.33 (*n* = 16)	745.13 ± 293.62 (*n* = 10)	753.74 ± 345.85 (*n* = 11)	778.11 ± 411.71 (*n* = 15)
Apparent looming threshold (rad s^{-1})	3.55 ± 2.29 (*n* = 18)	3.90 ± 3.70 (*n* = 12)	3.63 ± 2.16 (*n* = 15)	2.68 ± 2.05 (*n* = 19)
Maximum acceleration (cm s^{-2})	6109.23 ± 2156.49 (*n* = 18)	5659.69 ± 2412.32 (*n* = 13)	6031.76 ± 2088.32 (*n* = 16)	6053.00 ± 1736.15 (*n* = 19)
Maximum speed (cm s^{-1})	92.77 ± 28.54 (*n* = 18)	88.91 ± 33.35 (*n* = 13)	95.86 ± 30.33 (*n* = 16)	98.80 ± 29.88 (*n* = 19)
Cumulative distance (cm)	4.19 ± 1.32 (*n* = 18)	4.08 ± 1.72 (*n* = 13)	4.40 ± 1.55 (*n* = 16)	4.66 ± 1.34 (*n* = 19)

n, sample size; “0 ms”, “33 ms”, “83 ms” and “control” show 0 ms treatment, 33 ms treatment, 83 ms treatment, and control, respectively. Escape trajectories are expressed as circular-mean ± standard deviation (s.d.). Others are expressed as linear means ± s.d.